Probing entanglement and testing Bell inequality violation with $e^+e^- \to \tau^+\tau^-$ at Belle II

K. Ehatäht,[1] M. Fabbrichesi,[2] L. Marzola,[1] and C. Veelken[1]

[1]*Laboratory of High-Energy and Computational Physics, NICPB, Rävala puiestee 10, 10143 Tallinn, Estonia*

[2]*INFN, Sezione di Trieste, Via Valerio 2, I-34127 Trieste, Italy*

(Received 13 December 2023; accepted 19 January 2024; published 12 February 2024)

We present a feasibility study to probe quantum entanglement and Bell inequality violation in the process $e^+e^- \to \tau^+\tau^-$ at a center-of-mass energy of $\sqrt{s} = 10.579$ GeV. The sensitivity of the analysis is enhanced by applying a selection on the scattering angle ϑ in the $\tau^+\tau^-$ center-of-mass frame. We analyze events in which both τ leptons decay to hadrons, using a combination of decay channels $\tau^- \to \pi^-\nu_\tau$, $\tau^- \to \pi^-\pi^0\nu_\tau$, and $\tau^- \to \pi^-\pi^+\pi^-\nu_\tau$. The spin orientation of the τ leptons in these decays is reconstructed using the polarimeter-vector method. Assuming a dataset of 200 million $\tau^+\tau^-$ events and accounting for experimental resolutions, we expect the observation of quantum entanglement and Bell inequality violation by the Belle-II experiment will be possible with a significance well in excess of five standard deviations.

DOI: 10.1103/PhysRevD.109.032005

I. INTRODUCTION

The most distinctive feature of quantum mechanics is the inseparable nature of states describing physical systems that have interacted in the past. The entangled states give rise to correlations between these systems that are present even after they are separated and can no longer interact. After establishing the presence of quantum entanglement, observables testing the violation of Bell inequality [1] are the most interesting, because they provide a direct proof of the nonlocal nature of quantum correlations. The Bell inequality is derived by combining the probabilities of the outcome of various measurements between two observers under the assumption of Bell locality—that is, the factorizability of these probabilities with respect to all shared resources (see, for example, [2] for a review). Quantum mechanics does not satisfy Bell locality, and the inequality can, therefore, be violated.

Bell inequality violation has been verified experimentally with the polarizations of low-energy (that is, few eV) photons in [3,4]: Two photons are prepared into a singlet state and their polarizations measured along different directions to verify their entanglement and the violation of Bell inequality. Many experiments have been performed to further test the inequality [5,6] and close possible loopholes [7,8] with photons, using superconducting circuits [9] and using atoms [10]. The reader can find more details and references in two review articles [11,12].

Though the study of entangled states and Bell inequality has been an ongoing concern in atomic and solid-state physics for many years, it is only recently that also the high-energy community has taken up in earnest the study of the subject. Collider detectors, while not designed for the probing of entanglement, turn out to be surprisingly good in performing this task, thus ushering in the possibility of many interesting new measurements as well as new tools in probing physics beyond the Standard Model.

Entanglement with low-energy protons has been probed in Ref. [13] and proposed at colliders using hadronic final states in Ref. [14]. The higher energy probes quantum entanglement at smaller length scales [15]. Tests in the high-energy regime of particle physics have been suggested by means of neutral kaon physics [16–18] (see also Ref. [19]), positronium [20], flavor oscillations in neutral B mesons [21], charmonium decays [22], and neutrino oscillations [23]. A discussion of some of these issues also appears in Refs. [24,25]. The interest has been revived recently after entanglement has been argued [26] to be present in top-quark pair production at the LHC and it was shown [27] that Bell inequality violation is experimentally accessible in the same system. Following these works, the study of entanglement has been proposed for top-quark production [28–32], hyperons [33], and gauge bosons from

Higgs boson decay [34–37] and direct production [36,37]. For all these particles, it is possible to study entanglement and verify the violation of Bell inequality. Entanglement has recently been observed in top-quark pairs produced at a center-of-mass energy of $\sqrt{s} = 13$ TeV [38]. It has also been argued [39] that Bell inequality is violated in the decays of B mesons at LHCb and Belle II.

In this paper, we propose to probe quantum entanglement and Bell inequality violation using the process $e^+e^- \to \tau^+\tau^-$ at the Belle-II experiment, located at the SuperKEKB collider. The SuperKEKB collider delivers e^+e^- collisions at a center-of-mass (c.m.) energy of $\sqrt{s} = 10.579$ GeV. The Belle collaboration has published analyses of $e^+e^- \to \tau^+\tau^-$ production with data corresponding to an integrated luminosity of up to 921 fb^{-1}, equivalent to up to 841 million $\tau^+\tau^-$ events [40], while another 175 million events have been added with the Belle II dataset [41]. The final aim of the SuperKEKB project is to collect 50 ab^{-1} of data [42,43]. This would result in a dataset of about 50 billion $e^+e^- \to \tau^+\tau^-$ events.

We assess the feasibility of our proposal with a Monte Carlo (MC) study. The study is based on 200 million $e^+e^- \to \tau^+\tau^-$ events, which we analyze in three decay channels: $\tau^- \to \pi^-\nu_\tau$, $\tau^- \to \pi^-\pi^0\nu_\tau$, and $\tau^- \to \pi^-\pi^+\pi^-\nu_\tau$. The combination of these decay channels covers about 21% of τ pair decays. The detection of quantum entanglement and Bell inequality in the process $e^+e^- \to \tau^+\tau^-$ requires the measurement of τ spin correlations in the rest frames of the τ^+ and τ^-. Besides the availability of a large $\tau^+\tau^-$ dataset, our motivation for performing this study at Belle II is that the overconstrained event kinematics and comparatively low c.m. energy allow for a precise reconstruction of these rest frames, which, in turn, allows for a precise measurement of the τ spin correlations in the directions transverse and longitudinal to the τ flight direction. The measurement of transverse and longitudinal τ spin correlations is important in order to distinguish quantum entanglement from local hidden-variable theories [15].

Ours is the first study of entanglement and Bell inequality violation in the process $e^+e^- \to \tau^+\tau^-$ at Belle II. Tests of entanglement and Bell inequality violation in $\tau^+\tau^-$ systems has previously been proposed in e^+e^- collisions at LEP [44], pp collisions at the LHC [45], and at future leptonic colliders [46,47].

The paper is organized as follows: In Sec. II, we briefly summarize how the density matrix describing the polarization state of the τ pair can be computed from the amplitudes of the underlying process. Section III introduces the entanglement observables that we track in the following Monte Carlo analysis. In Sec. IV, we propose a strategy for detecting quantum entanglement and Bell inequality violation in the data recorded by the Belle-II experiment. The details and results pertaining to the performed numerical study are described in Sec. V, and our conclusions are offered in Sec. VI.

II. TAU SPIN CORRELATIONS IN THE STANDARD MODEL

The density matrix describing the polarization state of the bipartite system formed by the τ-lepton pair can be written as

$$\rho = \frac{1}{4}\left[\mathbb{1}\otimes\mathbb{1} + \sum_i \mathbf{B}_i^+(\sigma_i\otimes\mathbb{1}) + \sum_j \mathbf{B}_j^-(\mathbb{1}\otimes\sigma_j) + \sum_{i,j}\mathbf{C}_{ij}(\sigma_i\otimes\sigma_j)\right], \tag{2.1}$$

where $i, j \in \{n, r, k\}$ and σ_i are the Pauli matrices. The coefficients $\mathbf{B}_i^\pm$ encode the polarization of the corresponding $\tau^\pm$ lepton, whereas the matrix $\mathbf{C}_{ij}$ contains the polarization correlations. The proposed decomposition refers to a right-handed orthonormal basis $\{\hat{\mathbf{n}}, \hat{\mathbf{r}}, \hat{\mathbf{k}}\}$ [48] defined in the τ-pair center-of-mass frame as follows:

$$\hat{\mathbf{n}} = \frac{1}{\sin\vartheta}(\hat{\mathbf{p}}\times\hat{\mathbf{k}}), \qquad \hat{\mathbf{r}} = \frac{1}{\sin\vartheta}(\hat{\mathbf{p}} - \cos\vartheta\hat{\mathbf{k}}) \tag{2.2}$$

with $\hat{\mathbf{k}}$ being the direction of one of the τ leptons in the center-of-mass frame and ϑ the angle satisfying $\hat{\mathbf{p}}\cdot\hat{\mathbf{k}} = \cos\vartheta$, with $\hat{\mathbf{p}}$ an arbitrary unit vector in the production plane. The quantization axis for the polarization is taken along $\hat{\mathbf{k}}$, so that $\sigma_k \equiv \sigma_3$. Formally,

$$\mathbf{B}_i^+ = \mathrm{Tr}[\rho(\sigma_i\otimes\mathbb{1})], \tag{2.3}$$

$$\mathbf{B}_i^- = \mathrm{Tr}[\rho(\mathbb{1}\otimes\sigma_i)], \tag{2.4}$$

$$\mathbf{C}_{ij} = \mathrm{Tr}[\rho(\sigma_i\otimes\sigma_j)], \tag{2.5}$$

as implied by the properties $\mathrm{Tr}(\sigma_i\sigma_j) = 2\delta_{ij}$ and $\mathrm{Tr}(\sigma_i) = 0$.

The polarization density matrix can be computed from the scattering amplitude of the underlying $e^+e^- \to \tau^+\tau^-$ process in the following way. Consider the amplitude for the production of a fermion ψ_λ with polarization $\lambda \in \{-\frac{1}{2}, \frac{1}{2}\}$ along a given quantization direction:

$$\mathcal{M}(\lambda) = [\bar{u}_\lambda \mathcal{A}], \tag{2.6}$$

where the symbol $\mathcal{A}$ indicates the term in the amplitude $\mathcal{M}$ multiplying the spinor $\bar{u}_\lambda$ and square brackets denote a contraction of spinor indices. The outgoing particle is then described by a state

$$|\psi\rangle = \sum_\lambda \mathcal{M}(\lambda)|u_\lambda\rangle \tag{2.7}$$

yielding the spinor-space density matrix

$$\rho_\psi = \frac{|\psi\rangle\langle\psi|}{\langle\psi|\psi\rangle} = \frac{\sum_{\lambda\lambda'}[\bar{u}_\lambda \mathcal{A}][\bar{u}_{\lambda'}\mathcal{A}]^\dagger |u_\lambda\rangle\langle\bar{u}_{\lambda'}|}{\sum_{\lambda\lambda'}[\bar{u}_\lambda \mathcal{A}][\bar{u}_{\lambda'}\mathcal{A}]^\dagger \langle\bar{u}_{\lambda'}|u_\lambda\rangle} = \frac{\sum_{\lambda\lambda'}[\bar{u}_\lambda \mathcal{A}][\bar{u}_{\lambda'}\mathcal{A}]^\dagger |u_\lambda\rangle\langle\bar{u}_{\lambda'}|}{2m\sum_\lambda [\bar{u}_\lambda \mathcal{A}][\bar{u}_\lambda \mathcal{A}]^\dagger} = \frac{\sum_{\lambda\lambda'}[\mathcal{A}\bar{u}_{\lambda'}]^\dagger[\mathcal{A}\bar{u}_\lambda]|u_\lambda\rangle\langle\bar{u}_{\lambda'}|}{2m|\mathcal{M}|^2}, \tag{2.8}$$

where we made use of the orthogonality relation $\langle\bar{u}_{\lambda'}|u_\lambda\rangle \equiv [\bar{u}_{\lambda'}u_\lambda] = 2m\delta_{\lambda'\lambda}$ with m being the mass of the fermion and $|\mathcal{M}|^2$ the squared amplitude (summed over the spin) for the production process.

The density matrix in the polarization space can be obtained upon projection via the operators [49]

$$\frac{|u_\lambda\rangle\langle\bar{u}_{\lambda'}|}{2m} \equiv \frac{\Pi^u_{\lambda\lambda'}}{2m} = \frac{1}{4m}(\not{p}+m)\left(\delta_{\lambda\lambda'} + \gamma_5 \sum_i \not{s}_i \sigma^i_{\lambda\lambda'}\right), \tag{2.9}$$

$$\frac{|v_\lambda\rangle\langle\bar{v}_{\lambda'}|}{2m} \equiv \frac{\Pi^v_{\lambda\lambda'}}{2m} = \frac{1}{4m}(\not{p}-m)\left(\delta_{\lambda\lambda'} + \gamma_5 \sum_i \not{s}_i \sigma^i_{\lambda\lambda'}\right), \tag{2.10}$$

where $\{s_i^\mu\}$ is a triad of spacelike four-vectors, satisfying $s_i^\mu p_\mu = 0$, obtained by boosting the canonical basis[1] of the spin four-vector s to the frame where the fermion has four-momentum p. By acting with the first projector on the spinor-space density matrix, we then obtain

$$\rho_{\lambda\lambda'} = \left[\frac{\Pi^u_{\lambda\lambda'}}{2m}\rho_\psi\right] = \frac{[\mathcal{A}\mathcal{A}^\dagger \Pi^u_{\lambda\lambda'}]}{|\mathcal{M}|^2} = \frac{1}{2}\left(\mathbb{1} + \sum_i \langle s_i\rangle \sigma^i\right), \tag{2.11}$$

where $i \in \{n, r, k\}$ and $\langle X\rangle$ is the ensemble average of the quantity X. The computation of the density matrix for an antifermion $\bar{\psi}_\lambda$ proceeds analogously with the replacement of the projection operator in Eq. (2.9) by that of Eq. (2.10). The generalization to processes yielding more than one fermion in the final state is straightforward and recovers Eq. (2.1) for the pair production case. In particular, we have $\mathbf{B}_i^\pm = \langle s_i^\pm\rangle$ and $\mathbf{C}_{ij} = \langle s_i^+ s_j^-\rangle$, with s_i^+ and s_i^- being the spin vector of the antifermion and fermion, respectively.

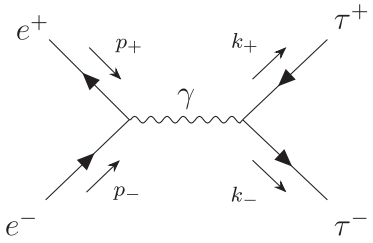

FIG. 1. The tree-level Feynman diagram for the considered process. We omit Z and H contributions as they are negligible at $\sqrt{s} = 10.579$ GeV.

The amplitude of the process we are interested in can be obtained from the diagram in Fig. 1, yielding

$$\mathcal{M} = -\frac{e^2}{s}[\bar{v}(p_+)\gamma^\mu u(p_-)][\bar{u}(k_-)\gamma_\mu v(k_+)], \tag{2.12}$$

where $s = (p_+ + p_-)^2$ and the squared amplitude

$$|\mathcal{M}|^2 = \frac{4e^4}{s}(4m_\tau^2 \sin^2\vartheta + s(\cos^2\vartheta + 1)), \tag{2.13}$$

where we neglected the mass of the electron and summed over the spin of all the involved fermions. In the τ-pair center-of-mass frame, our conventions set $\hat{\mathbf{k}}$ along the k_+ momentum and $\hat{\mathbf{p}}$ along p_+ and identify the angle ϑ in Eq. (2.2) with the scattering angle included by these momenta.

Computing the polarization density matrix of the τ pair, we find

$$\rho = r_0 \begin{pmatrix} s(\cos^2\vartheta+1) & -i\sqrt{s}m_\tau \sin 2\vartheta & -i\sqrt{s}m_\tau \sin 2\vartheta & -s\sin^2\vartheta \\ i\sqrt{s}m_\tau \sin 2\vartheta & 4m_\tau^2\sin^2\vartheta & 4m_\tau^2\sin^2\vartheta & i\sqrt{s}m_\tau \sin 2\vartheta \\ i\sqrt{s}m_\tau \sin 2\vartheta & 4m_\tau^2\sin^2\vartheta & 4m_\tau^2\sin^2\vartheta & i\sqrt{s}m_\tau \sin 2\vartheta \\ -s\sin^2\vartheta & -i\sqrt{s}m_\tau \sin 2\vartheta & -i\sqrt{s}m_\tau \sin 2\vartheta & s(\cos^2\vartheta+1) \end{pmatrix}, \tag{2.14}$$

where $r_0 = 1/(8m_\tau^2\sin^2\vartheta + 2s(\cos^2\vartheta+1))$.

[1] In the rest frame of the fermion, we have $s = (0, \mathbf{s})$ and

$$s_1 = \begin{pmatrix} 0 \\ 1 \\ 0 \\ 0 \end{pmatrix}, \qquad s_2 = \begin{pmatrix} 0 \\ 0 \\ 1 \\ 0 \end{pmatrix}, \qquad s_3 = \begin{pmatrix} 0 \\ 0 \\ 0 \\ 1 \end{pmatrix}.$$

For the coefficients in Eq. (2.1), we obtain $\mathbf{B}_i^{\pm} = 0$ and

$$\mathbf{C} = c_0 \begin{pmatrix} (4m_\tau^2 - s)\sin^2\vartheta & 0 & 0 \\ 0 & (4m_\tau^2 + s)\sin^2\vartheta & 4m_\tau\sqrt{s}\sin\theta\cos\vartheta \\ 0 & 4m_\tau\sqrt{s}\sin\vartheta\cos\vartheta & -4m_\tau^2\sin^2\vartheta + s(\cos^2\vartheta + 1) \end{pmatrix}, \tag{2.15}$$

where $c_0 = 1/(4m_\tau^2\sin^2\vartheta + s(\cos^2\vartheta + 1))$. Averaging over the angular distribution of the two τ leptons yields

$$\langle \mathbf{C} \rangle = \begin{pmatrix} -0.419875 & 0 & 0 \\ 0 & 0.526708 & 0 \\ 0 & 0 & 0.893167 \end{pmatrix} \tag{2.16}$$

for $\sqrt{s} = 10.579$ GeV and $m_\tau = 1.777$ GeV.

Equation (2.16) shows that the parameter $D = \mathrm{Tr}(\langle \mathbf{C} \rangle)/3 = 1/3$ does not signal the presence of entanglement, as it relies on an average. Averaging, in general, dilutes the effect of quantum correlations.

III. ENTANGLEMENT OBSERVABLES

On general grounds, a bipartite state is called *separable* if its density matrix can be written as a convex combination of product states:

$$\rho_{\mathrm{sep}} = \sum_{i,j} p_{ij}\rho_i^A \otimes \rho_j^B, \quad \text{with} \quad p_{ij} > 0 \quad \text{and} \quad \sum_{i,j} p_{ij} = 1, \tag{3.1}$$

where the labels A and B denote the two composing subsystems. By definition, a system is called *entangled* if it is *not* separable.

Quantifying the entanglement content of a bipartite system is generally a complicated task, because the possible decompositions into pure state pose an optimization problem for the chosen entanglement measure or monotone. Fortunately, algebraic solutions are available for simpler systems, for instance, for those composed of two qubits. In order to assess the presence of entanglement in the τ-pair polarization state, we track the *concurrence* $\mathcal{C}[\rho]$ [50–52], an entanglement monotone which for a bipartite qubit system can be quantified as

$$\mathcal{C}[\rho] = \max\{0, \lambda_1 - \lambda_2 - \lambda_3 - \lambda_4\} \in [0, 1], \tag{3.2}$$

where λ_i are the eigenvalues, in decreasing order, of the matrix

$$R = \sqrt{\sqrt{\rho}\tilde{\rho}\sqrt{\rho}}, \quad \text{with} \quad \tilde{\rho} = (\sigma_2 \otimes \sigma_2)\rho^*(\sigma_2 \otimes \sigma_2). \tag{3.3}$$

Nonvanishing values of the concurrence witness the presence of entanglement, and a value of 1 indicates a maximally entangled state. At the tree level, we find

$$\mathcal{C}[\rho] = \frac{(s - 4m_\tau^2)\sin^2\vartheta}{4m_\tau^2\sin^2\vartheta + s(\cos^2\vartheta + 1)} \tag{3.4}$$

for the process $e^+e^- \to \tau^+\tau^-$. Entanglement vanishes at the kinematic threshold, because the conservation of angular momentum, in the absence of an orbital component, forces the complete classical correlation of the τ-pair spins and their state into a separable one.

The genuine quantum correlations that entangle the polarization states of the τ lepton can also be used to discriminate between quantum mechanics and alternative local stochastic classical theories relying on hidden variables [53]. This is the idea behind the so-called Bell inequalities [1], which bound the expectation value of a suitable operator under the hypothesis that the involved correlators are *local*, i.e., that they factorize according to the rules of probability [44]. For the bipartite qubit system at hand, a useful test is encoded in the following inequality [5]:

$$|\hat{n}_1 \cdot \mathbf{C} \cdot (\hat{n}_2 - \hat{n}_4) + \hat{n}_3 \cdot \mathbf{C} \cdot (\hat{n}_2 + \hat{n}_4)| \leq 2, \tag{3.5}$$

with $\hat{n}_i$ being four unit vectors indicating the directions along which the spins of the two leptons can be measured. The upper bound is respected by correlations stemming from local theories but *can* be violated within quantum mechanics if the state of interest is entangled. In order to detect the violation of this generalized Bell inequality, it is necessary to maximize the effect through a suitable choice of the four measurement directions. The procedure can be bypassed by introducing the operator $\mathfrak{m}_{12}[\mathbf{C}]$ [54], defined as

$$\mathfrak{m}_{12}[\mathbf{C}] = m_1 + m_2, \tag{3.6}$$

where $m_1 \geq m_2 \geq m_3$ are the eigenvalues of the positive semidefinite matrix $M = \mathbf{C}^T\mathbf{C}$. If and only if $\mathfrak{m}_{12}[\mathbf{C}] > 1$, then the bound in Eq. (3.5) is violated and local hidden-variable theories can be ruled out.

With the results in Eq. (2.15), we find

$$\mathfrak{m}_{12}[\mathbf{C}] = 1 + \left(\frac{(s - 4m_\tau^2)\sin^2\vartheta}{4m_\tau^2\sin^2\vartheta + s(\cos^2\vartheta + 1)}\right)^2, \tag{3.7}$$

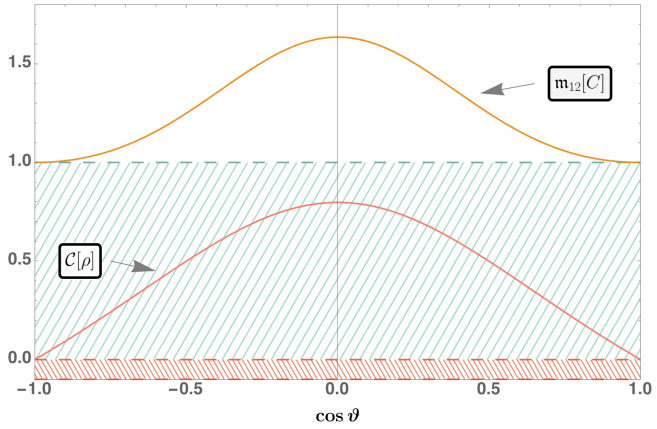

FIG. 2. The observables $\mathfrak{m}_{12}[\mathbf{C}]$ and $\mathcal{C}[\rho]$ as a function of the scattering angle ϑ (defined by the directions of the incoming positron and outgoing τ^+ in the τ-pair rest frame) at $\sqrt{s} = 10.579$ GeV. The solid red and yellow lines represent the Standard Model expectation for these observables. Entanglement is present if $\mathcal{C}[\rho] > 0$ (above the area hatched in red), while the generalized Bell inequalities are violated for $\mathfrak{m}_{12}[\mathbf{C}] > 1$ (above the area hatched in green). For both observables, the central region (for small $\cos\vartheta$) is where the largest values are to be found.

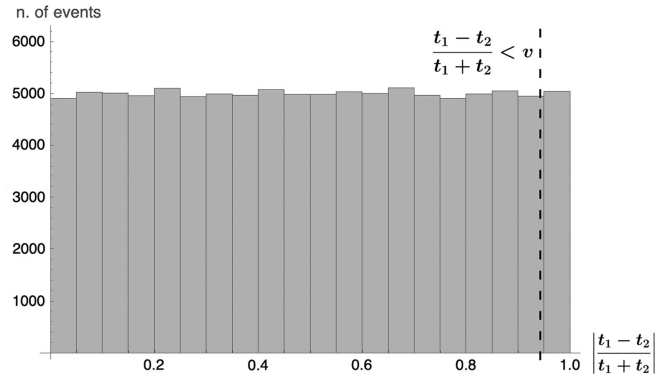

FIG. 3. Histogram of the number of events as a function of the ratio $|t_1 - t_2|/(t_1 + t_2)$ between the difference and the sum of the decay times of the two taus. The events have been generated by 10^5 pseudoexperiments in which the decay times are randomly varied within an exponential distribution. The black-dashed vertical line distinguishes events separated by a timelike interval (to the right of the line) from those that are spacelike separated (to the left of the line).

which we plot in Fig. 2 as a function of the scattering angle. The figure shows that the violation of the bound in Eq. (3.5) becomes easier to detect when one selects events in which the τ pair is produced in direction transverse to the beam axis.

In relation to the proposed Bell test, we remark that the relative velocity v with which the τ pair flies apart is sufficiently large to create, at the times t_1 and t_2 of decay, a spacelike separation

$$\frac{|t_1 - t_2|c}{(t_1 + t_2)v} < 1, \tag{3.8}$$

for more than 95% of the τ pairs (see Fig. 3). The separation prevents local interactions (as those arising through the exchange of photons between the charged taus) and ensures that the locality loophole [55] is closed. The selection of these events could be implemented with a suitable cut on the relative momentum of the two particles. However, given the amount of available data and the small fraction of pairs rejected by the cut, this refinement would not affect the significance of the proposed Bell test.

IV. MEASUREMENT OF TAU SPIN CORRELATIONS

The measurement of the τ spin correlation matrix $\mathbf{C}$ is based on the spin-dependent differential cross section $d\sigma$ for the process $e^+e^- \to \tau^+\tau^-$, which is given by [56]

$$d\sigma = |\bar{\mathcal{M}}_p|^2(1 - b_\mu^+ s_+^\mu - b_\nu^- s_-^\nu + c_{\mu\nu} s_+^\mu s_-^\nu) d\text{Lips}, \tag{4.1}$$

where $|\bar{\mathcal{M}}_p|^2$ denotes the spin-averaged matrix element for the process $e^+e^- \to \tau^+\tau^-$ and dLips is the Lorentz invariant phase-space measure. The symbols s_+^μ and s_-^μ refer to the spin of the τ^+ and of the τ^-. Combining Eq. (4.1) with the expression for the differential decay rate of the τ, given by [56]

$$d\Gamma = \frac{1}{2m_\tau}|\bar{\mathcal{M}}_d|^2(1 + h_\mu s^\mu) d\text{Lips}, \tag{4.2}$$

one obtains the relation

$$d\sigma = |\bar{\mathcal{M}}_p|^2|\bar{\mathcal{M}}_d|^2|\bar{\mathcal{M}}'_d|^2(1 - b_\mu^+ h_+^\mu - b_\nu^- h_-^\nu + c_{\mu\nu} h_+^\mu h_-^\nu) d\text{Lips}. \tag{4.3}$$

The symbols $|\bar{\mathcal{M}}_d|^2$ and $|\bar{\mathcal{M}}'_d|^2$ refer to the spin-averaged matrix elements for the decay of the τ^+ and τ^-, and h_+^μ and h_-^ν denote the polarimeter vectors of the τ^+ and τ^-, respectively. The polarimeter vectors provide a handle to measure the orientation of the τ^+ and τ^- spins. The relation between the polarimeter vector and the τ spin orientation is given by Eq. (4.2).

For the three decay channels $\tau^- \to \pi^-\nu_\tau$, $\tau^- \to \pi^-\pi^0\nu_\tau$, and $\tau^- \to \pi^-\pi^+\pi^-\nu_\tau$ considered in this paper, the polarimeter vector is a function of the momenta of the charged and neutral pions produced in the τ decay. For the decay channels $\tau^- \to \pi^-\nu_\tau$ and $\tau^- \to \pi^-\pi^0\nu_\tau$, the polarimeter vector can be computed analytically, and we use the expressions given by Eqs. (3.25) and (3.39) in Ref. [56]. For the decay channel $\tau^- \to \pi^-\pi^+\pi^-\nu_\tau$, it is not possible to derive analytic expressions for the polarimeter vector, and we instead use the algorithm in Ref. [57] to compute h_+^μ and h_-^ν numerically. The decays $\tau^- \to \pi^-\pi^0\nu_\tau$ and $\tau^- \to \pi^-\pi^+\pi^-\nu_\tau$ proceed via intermediate $\rho(770)$ and $a_1(1260)$

resonances. We, hence, refer to these decay channels as π^+, ρ^+, and a_1^+ for the τ^+ and as π^-, ρ^-, and a_1^- for the τ^-.

It has been shown that all hadronic τ decay channels provide the same sensitivity, or "τ spin analyzing power," if the charged and neutral pions produced in the τ decays can be reconstructed and measured with negligible experimental resolution [58]. In contrast, the spin analyzing power of the leptonic decay channels $\tau^- \to e^- \bar{\nu}_e \nu_\tau$ and $\tau^- \to \mu^- \bar{\nu}_\mu \nu_\tau$ is limited to about 40% compared to hadronic τ decays [59]. For this reason, we focus on hadronic τ decays in this paper.

The polarimeter vectors h_+^μ and h_-^ν need to be computed in the rest frames of the τ^+ and τ^-. The rest frames are determined by reconstructing the full event kinematics, including the momenta of the two neutrinos produced in the τ decays, as detailed in the next section. In the τ^+ and τ^- rest frames, the timelike component of the polarimeter vector vanishes: $h^0 = 0$. Equation (4.3) thus reduces to

$$d\sigma = |\bar{\mathcal{M}}_p|^2 |\bar{\mathcal{M}}_d|^2 |\bar{\mathcal{M}}'_d|^2 (1 + \mathbf{B}^+ \cdot \mathbf{h}^+ + \mathbf{B}^- \cdot \mathbf{h}^- + \mathbf{h}^+ \cdot \mathbf{C} \cdot \mathbf{h}^-) d\mathrm{Lips}. \tag{4.4}$$

Using this relation, we determine the polarizations $\mathbf{B}^+$ and $\mathbf{B}^-$ and the spin correlation matrix $\mathbf{C}$ by an unbinned maximum-likelihood (ML) fit [60]. The likelihood function is given by

$$\mathcal{L} = \prod_i (1 + \mathbf{B}^+ \cdot \mathbf{h}_i^+ + \mathbf{B}^- \cdot \mathbf{h}_i^- + \mathbf{h}_i^+ \cdot \mathbf{C} \cdot \mathbf{h}_i^-). \tag{4.5}$$

In Eq. (4.5), the subscript i refers to the events i in the $e^+e^- \to \tau^+\tau^-$ event sample, and the product extends over all events in this sample. The 15 parameters of the fit—the three elements of the polarization vector $\mathbf{B}^+$ of the τ^+, the three elements of the polarization vector $\mathbf{B}^-$ of the τ^-, and the nine elements of the spin correlation matrix $\mathbf{C}$—are determined by a numerical maximization of the likelihood function $\mathcal{L}$ with respect to these parameters. The parameters are expressed in the $\{\hat{\mathbf{n}}, \hat{\mathbf{r}}, \hat{\mathbf{k}}\}$ coordinate system defined in Sec. II. The maximization is performed numerically, using the program MINUIT [61]. Alternative procedures for determining $\mathbf{B}^+$, $\mathbf{B}^-$, and $\mathbf{C}$ are compared to the ML-fit method in Appendix B.

Equation (4.4) holds for a fixed value of the scattering angle ϑ. We have checked that the maximization of the likelihood function yields an unbiased estimate of the spin correlation matrix $\mathbf{C}$ when Eq. (2.15) is integrated over intervals in ϑ. As an example, we give in Eq. (4.6) the spin correlation matrix computed for a sample of $e^+e^- \to \tau^+\tau^-$ events, produced by MC simulation as detailed in Sec. V:

$$\mathbf{C} = \begin{pmatrix} -0.4129 \pm 0.0033 & -0.0014 \pm 0.0040 & 0.0008 \pm 0.0036 \\ 0.0007 \pm 0.0029 & 0.5273 \pm 0.0032 & 0.0024 \pm 0.0030 \\ 0.0024 \pm 0.0031 & 0.0030 \pm 0.0032 & 0.8829 \pm 0.0028 \end{pmatrix}. \tag{4.6}$$

The events considered in the computation were selected in the decay channel $\pi^+\pi^-$ within the range $0 \le \vartheta \le \pi$ and were analyzed on MC-truth level. No selection criteria (acceptance cuts) are applied on the charged and neutral pions produced in the τ decays. All nine elements of the matrix agree with the Standard Model expectation, given by Eq. (2.16), within the quoted statistical uncertainties.

Once the spin correlation matrix $\mathbf{C}$ is determined, we compute the observables $\mathcal{C}[\rho]$ and $\mathfrak{m}_{12}[\mathbf{C}]$ using Eqs. (3.2) and (3.6), in order to test for entanglement and Belle inequality violation. The elements of the density matrix ρ are given by $\mathbf{B}^+$, $\mathbf{B}^-$, and $\mathbf{C}$ through Eq. (2.1).

Figure 2 demonstrates that the feasibility to detect quantum entanglement and Belle inequality violation increases if one selects events in which the τ leptons are produced in direction transverse to the beam axis, i.e., with $\vartheta \approx \pi/2$. We perform an optimization of a selection on ϑ, with the aim of maximizing the significances $\mathcal{C}[\rho]/\delta\mathcal{C}[\rho]$ and $(\mathfrak{m}_{12}[\mathbf{C}] - 1)/\delta\mathfrak{m}_{12}[\mathbf{C}]$. The results of this optimization will be presented in the next section.

V. MONTE CARLO STUDY

A sample of 200 million $e^+e^- \to \tau^+\tau^-$ MC events was generated with the program MadGraph_aMC@NLO v2.9.16 [62], using leading-order matrix elements. The program PYTHIA v8.306 [63] is used for the modeling of parton showers, hadronization processes, and τ decays. All τ decay channels are included in the simulation. The events are analyzed on MC-truth level and after taking realistic experimental resolutions into account.

Instead of performing a full simulation of the Belle-II detector [64] based on Geant4 [65], we simulate the experimental resolution by randomly varying ("smearing") the position of the primary event vertex, the four-vectors of the charged and neutral particles produced in the τ decays, and the longitudinal (d_{xy}) and transverse (d_z) impact parameters of tracks. In the case of τ decays into three charged pions, we also smear the position of the τ decay vertex. The z axis is defined as the direction of the electron beam. For the τ decay channels considered in this paper, only the resolutions for charged pions ($\pi^\pm$) and

TABLE I. Experimental resolutions used in the MC study.

Charged hadrons	
Quantity	Resolution
p_T: c_0	1×10^{-3} GeV^{-1}
p_T: c_1	3×10^{-3}
θ	10^{-3}
ϕ	10^{-3}
d_{xy}	10 μm
d_z	20 μm
Photons	
Quantity	Resolution
E: c_0	2×10^{-3} GeV
E: c_1	1.6×10^{-2} $\sqrt[4]{\text{GeV}}$
E: c_2	1.2×10^{-2}
θ	$4 \times 10^{-3}/\sqrt{E[\text{GeV}]}$
ϕ	$4 \times 10^{-3}/\sqrt{E[\text{GeV}]}$
Event vertex	
Quantity	Resolution
x	10 μm
y	10 μm
z	20 μm
$\tau^+\tau^-$ system	
Quantity	Resolution
p_x	0.01 GeV
p_y	0.01 GeV
p_z	0.1 GeV
Mass	0.1 GeV

for photons (γ) are relevant. The latter originate from neutral pion (π^0) decays. The resolutions are taken from Ref. [64] and are summarized in Table I. For the τ decay vertex, we assume a resolution of 500 μm in the direction parallel to the τ flight direction and 10 μm in each of the two perpendicular directions. The smeared values are obtained by randomly sampling from a Gaussian distribution with mean equal to the true value and width equal to the experimental resolution given in the table. The symbol p_T refers to the momentum in direction transverse to the beam axis, and the symbols θ and ϕ denote the polar and azimuthal angles, respectively, with respect to this axis. The resolution on the p_T of charged pions is parametrized by $\sigma_{p_T} = p_T(c_0 p_T \oplus c_1/\beta)$, where $\beta = \sqrt{1-(m/E)^2}$ is the charged pions' velocity in units of the speed of light. The resolution on the energy E of photons is parametrized by $\sigma_E = E(c_0/E \oplus c_1/\sqrt[4]{E} \oplus c_2)$. The coefficients c_i are given in Table I. The symbol $\oplus$ indicates that contributions to the resolutions are added in quadrature. Angular resolutions are given in units of radians. The angular resolution for $\pi^\pm$ represents our estimate. The angular resolution for γ improves proportional to the square root of the photons' energy. For the resolutions on the transverse and longitudinal impact parameters, which typically vary with p_T and θ of the track, we have taken averages and rounded the values to one significant digit. The energy spread of the beam electrons and the effect of beamstrahlung is simulated by varying the constraint on the energy of the $\tau^+\tau^-$ system and of its momentum in beam direction by 0.1 GeV [42] and by varying its momentum in direction transverse to the beam axis by 0.01 GeV.

The $\pi^\pm$ and γ produced in the τ decays are required to pass selection criteria, which ensure that the particles can be well identified and their momenta be well reconstructed in the Belle-II detector. Charged pions are required to have a transverse momentum $p_T > 0.1$ GeV, while photons are required to have an energy $E > 0.1$ GeV. Both are required to be within the geometric acceptance of the central drift chamber: $17 < \theta < 150°$. The selection criteria are taken from Ref. [40]. We refer to them as acceptance cuts.

The full kinematics of each event, including the momenta of the two neutrinos produced in the τ decays, is reconstructed using a two-step procedure. In the first step, we determine approximate values of the τ lepton momenta by solving a set of analytic equations. The approximate values are then used as starting point for a kinematic fit (KF), which is executed in the second step.

The first step is based on the formalism introduced in Appendix C in Ref. [46] and has been extended to the case of τ decay channels other than $\tau^+\tau^- \to \pi^+\bar{\nu}_\tau\pi^-\nu_\tau$. Details of the extended formalism are given in Appendix A.

The KF is based on the work presented in Refs. [66–68]. The number of fitted parameters totals 17: the position of the primary event vertex (3); the components p_x and p_y of the momenta of the neutrinos produced in the decay of the τ^+ and τ^- (4); the position of the decay vertices of τ^+ and τ^- (6); and the E, p_x, p_y, and mass components of the $\tau^+\tau^-$ system (4). For the uncertainties on these parameters, the KF uses the values given in Table I. We use the symbols τ_h^+ and τ_h^- to refer to the system of $\pi^\pm$ and γ produced in the decays of the τ^+ and τ^-, respectively. We assume the uncertainties on the $\pi^\pm$ and γ momenta to be negligible and, thus, do not include the τ_h^+ and τ_h^- momenta as parameters in the fit. For τ leptons that decay into $\pi^\pm$ or $\rho^\pm$, we follow the approach referred to as "huge error method" in Ref. [69] to allow the fit to freely vary the position of the τ decay vertex along the direction of the charged pion's track. The E and p_z components of the neutrino four-vector are computed analytically, using the τ and neutrino mass constraints. All other constraints are represented by Lagrange multipliers in the KF. In total, there are eight such constraints: four "parallelism" constraints of the type described in Sec. IV.1.3.3 in Ref. [67] and four constraints

that demand that the sum of $\tau_h^+ + \nu_\tau + \tau_h^- + \bar{\nu}_\tau$ four-vectors equals the four-vector of the e^+e^- initial state.

For the optimization of the selection on $|\cos(\vartheta)| < x$, we perform a scan of the significances $\mathcal{C}[\rho]/\delta\mathcal{C}[\rho]$ and $(\mathfrak{m}_{12}[\mathbf{C}] - 1)/\delta\mathfrak{m}_{12}[\mathbf{C}]$ as a function of the upper limit x, where the symbols $\delta\mathcal{C}[\rho]$ and $\delta\mathfrak{m}_{12}[\mathbf{C}]$ refer to the statistical uncertainties on the observables $\mathcal{C}[\rho]$ and $\mathfrak{m}_{12}[\mathbf{C}]$, respectively. We vary x within the range 0–1 in steps of 0.05. The result of the scan is illustrated in Fig. 4 for the cases that the event kinematics and polarimeter vectors are taken from MC-truth level and for the case that they are reconstructed by the KF after smearing the events by the experimental resolutions. A good compromise between maximizing the effect of entanglement and Bell inequality violation, on the one hand, and maintaining a high-statistics event sample, on the other hand, is achieved for the selection $|\cos(\vartheta)| < 0.40$. Maintaining a high-statistics event sample reduces the uncertainties $\delta\mathcal{C}[\rho]$ and $\delta\mathfrak{m}_{12}[\mathbf{C}]$.

In the figure, one can see that all decay channels contribute in a meaningful way to the sensitivity for detecting quantum entanglement and Bell inequality violation. The decay channels $\rho^+\rho^-$ and $\pi^\pm\rho^\mp$ contribute the most, reflecting their higher branching fractions. The significance of the combination is computed by adding the significances of individual decay channels in quadrature. The significances $\mathcal{C}[\rho]/\delta\mathcal{C}[\rho]$ and $(\mathfrak{m}_{12}[\mathbf{C}] - 1)/\delta\mathfrak{m}_{12}[\mathbf{C}]$ are reduced by about 10% and 30%, respectively, when the events are smeared by the experimental resolutions and reconstructed by the KF, compared to the sensitivity obtained at MC-truth level.

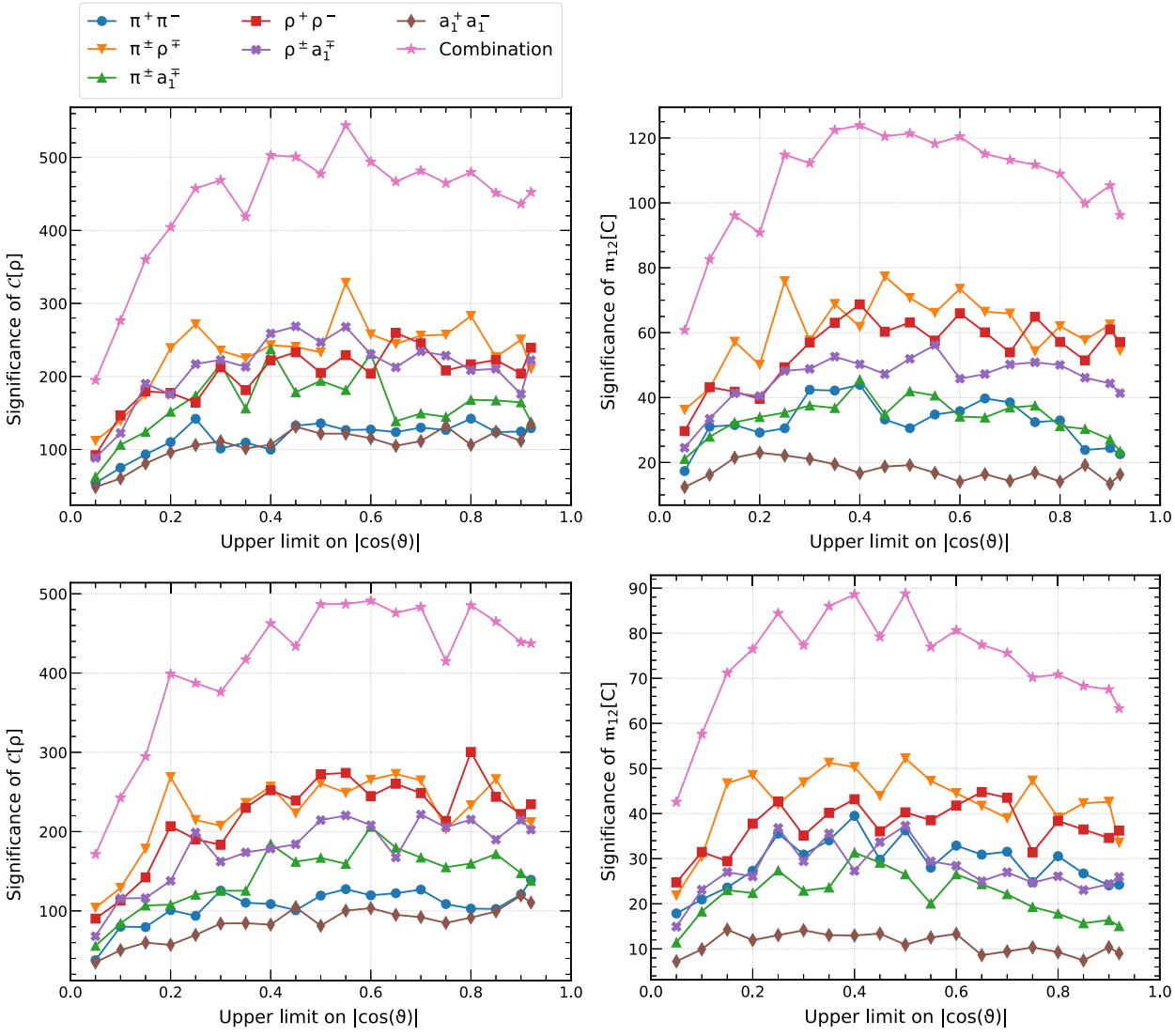

FIG. 4. Significances $\mathcal{C}[\rho]/\delta\mathcal{C}[\rho]$ (left) and $(\mathfrak{m}_{12}[\mathbf{C}] - 1)/\delta\mathfrak{m}_{12}[\mathbf{C}]$ (right) as a function of the upper limit imposed on $|\cos(\vartheta)|$. The significances are given for the decay channels $\pi^+\pi^-$, $\pi^\pm\rho^\mp$, $\pi^\pm a_1^\mp$, $\rho^\pm\rho^\mp$, $\rho^\pm a_1^\mp$, and $a_1^+a_1^-$ individually and for their combination. The events are analyzed on MC-truth level (top) and with experimental resolutions taken into account (bottom). No acceptance cuts are applied on the $\pi^\pm$ and γ produced in the τ decays.

TABLE II. Observables $\mathcal{C}[\rho]$ and $\mathfrak{m}_{12}[\mathbf{C}]$ measured in individual decay channels and for the combination of all six channels, for events that pass the acceptance cuts and the selection $|\cos(\vartheta)| < 0.40$. Events are analyzed on MC-truth level.

Decay channel	$\mathcal{C}[\rho]$	$\mathfrak{m}_{12}[\mathbf{C}]$
$\pi^+\pi^-$	0.7079 ± 0.0071	1.483 ± 0.011
$\pi^\pm\rho^\mp$	0.7113 ± 0.0029	1.482 ± 0.008
$\pi^\pm a_1^\mp$	0.6762 ± 0.0028	1.388 ± 0.009
$\rho^+\rho^-$	0.7111 ± 0.0032	1.495 ± 0.007
$\rho^\pm a_1^\mp$	0.6798 ± 0.0026	1.402 ± 0.008
$a_1^+ a_1^-$	0.6386 ± 0.0060	1.294 ± 0.018
All channels	0.6905 ± 0.0014	1.444 ± 0.004

Values and uncertainties on the observables $\mathcal{C}[\rho]$ and $\mathfrak{m}_{12}[\mathbf{C}]$ for events that pass the selection $|\cos(\vartheta)| < 0.40$ on the scattering angle ϑ are given in Tables II and III. Table II gives the results obtained when events are analyzed at MC-truth level and Table III those obtained after smearing the events by the experimental resolutions and reconstructing the event kinematics by the KF.

The uncertainties on $\mathbf{B}^+$, $\mathbf{B}^-$, and $\mathbf{C}$ as well as on the observables $\mathcal{C}[\rho]$ and $\mathfrak{m}_{12}[\mathbf{C}]$ are computed by bootstrapping [70]: A set of $N_{\text{toy}} = 100$ toy datasets is constructed from the original sample. The events in each toy dataset are drawn randomly from the original sample, such that the number of events in each toy dataset equals N. The bootstrap samples may contain the same event exactly once, multiple times, or not at all. The probability $P(n)$ for a certain event to be contained n times in the toy dataset is given by the Poisson distribution $P(n) = (\lambda^n e^{-\lambda})/n!$ with $\lambda = 1/N$. For each toy dataset, we compute the spin correlation matrix $\mathbf{C}$ by maximizing the likelihood function $\mathcal{L}$ given by Eq. (4.5). The statistical uncertainty on the element $\mathbf{C}_{ij}$ is then computed by sorting the N_{toy} values of this element, which we obtained by the bootstrapping procedure, and taking half the difference between the 84% and 16% quantiles. Statistical uncertainties on the observables $\mathcal{C}[\rho]$ and $\mathfrak{m}_{12}[\mathbf{C}]$ are estimated by taking the set of N_{toy} spin correlation matrices $\mathbf{C}$, computing $\mathcal{C}[\rho]$ and $\mathfrak{m}_{12}[\mathbf{C}]$ for each matrix using Eqs. (3.2) and (3.6), and then taking half the difference between the 84% and 16% quantiles for these observables.

TABLE III. Observables $\mathcal{C}[\rho]$ and $\mathfrak{m}_{12}[\mathbf{C}]$ measured in individual decay channels and for the combination of all six channels, for events that pass the acceptance cuts and the selection $|\cos(\vartheta)| < 0.40$. Events are reconstructed by the KF after smearing them by the experimental resolutions given in Table I.

Decay channel	$\mathcal{C}[\rho]$	$\mathfrak{m}_{12}[\mathbf{C}]$
$\pi^+\pi^-$	0.6722 ± 0.0062	1.463 ± 0.012
$\pi^\pm\rho^\mp$	0.6658 ± 0.0026	1.361 ± 0.007
$\pi^\pm a_1^\mp$	0.6370 ± 0.0035	1.298 ± 0.009
$\rho^+\rho^-$	0.6524 ± 0.0026	1.326 ± 0.008
$\rho^\pm a_1^\mp$	0.6181 ± 0.0035	1.264 ± 0.010
$a_1^+ a_1^-$	0.6062 ± 0.0073	1.229 ± 0.018
All channels	0.6475 ± 0.0014	1.331 ± 0.004

The values and uncertainties for the combination of decay channels in Tables II and III are computed by taking a weighted average of the individual decay channels i, with weights given by the inverse of the square of the uncertainties $\delta\mathcal{C}[\rho]_i$ and $\delta\mathfrak{m}_{12}[\mathbf{C}]_i$ expected for channel i. For the combination of all six decay channels, we expect that a measurement of τ spin correlations in the process $e^+e^- \to \tau^+\tau^-$ at Belle II will allow one to observe entanglement and Bell inequality violation with significances well in excess of five standard deviations (s.d.). The numerical values of the significances amount to 463 s.d. in case of entanglement and 87 s.d. in the case of Bell inequality violation.

The significances computed based on the numbers given in Tables II and III are about 10% lower compared to those shown in Fig. 4. The difference is due to the acceptance cuts. Events passing the selection $|\cos(\vartheta)| < 0.40$ pass the acceptance cuts with an efficiency that varies between 52% and 95%, depending on the τ decay channel. The effect of these efficiencies is to increase the uncertainties $\delta\mathcal{C}[\rho]$ and $\delta\mathfrak{m}_{12}[\mathbf{C}]$. The efficiency is the lowest for the decay channel $\rho^+\rho^-$ and the highest for the decay channel $\pi^+\pi^-$. We have checked that the acceptance cuts do not introduce a bias on the τ spin correlation. The values of $\mathcal{C}[\rho]$ and $\mathfrak{m}_{12}[\mathbf{C}]$ obtained for events passing the selection $|\cos(\vartheta)| < 0.40$ change only marginally, by about 1%, when the acceptance cuts are applied.

As can be seen by comparing Tables II and III, the experimental resolutions increase the uncertainties $\delta\mathcal{C}[\rho]$ and $\delta\mathfrak{m}_{12}[\mathbf{C}]$ by a small amount and also reduce the measured values and, thus, the significances by a few percent. As the focus of this study is the detection of entanglement and Bell inequality violation and not the precise measurement of $\mathcal{C}[\rho]$ and $\mathfrak{m}_{12}[\mathbf{C}]$, we do not make an attempt to mitigate this effect by accounting for the experimental resolutions in the likelihood function $\mathcal{L}$ given by Eq. (4.5) or compensate for the effect via calibration.

We advise the reader not to take the quoted values of the significances literally. We quote their numerical values solely for the purpose of substantiating our expectation that an observation of entanglement and Bell inequality violation with a significance well in excess of five s.d. is highly likely after all experimental effects, including effects not considered in our Monte Carlo study, are taken into account. The following three effects will degrade the sensitivity somewhat in a realistic experiment: the presence of non-Gaussian tails in the experimental resolutions, the presence of backgrounds, and systematic uncertainties. Of the three, the presence of backgrounds will probably have the most sizable effect.

Based on Fig. 1 in Ref. [41], we expect the dominant background to arise from misreconstruction of the τ decay channel. The figure shows that the τ decay channel gets misreconstructed in about 15% of $e^+e^- \to \tau^+\tau^-$ events at Belle II, while in the remaining 85% of events the τ decay channel is reconstructed correctly. Backgrounds arising from the process $e^+e^- \to q\bar{q}$ and from other sources are small in comparison. The misreconstruction of the τ decay channel may happen if, for example, the γ produced in π^0 decays fail to get reconstructed due to detection inefficiencies, are outside of the geometric acceptance of the electromagnetic calorimeter, or have energies below the threshold of 0.1 GeV. In the case the τ decay channel does get misreconstructed, two things happen: Because the polarimeter vector of the τ depends on the momenta of the particles produced in the τ decay in a way that is specific to each τ decay channel, the polarimeter vector will be computed in the wrong way. Besides, the wrong four-vectors will be used in that computation. Unfortunately, the full Belle-II detector simulation based on Geant4 [65] is necessary to study the misreconstruction of the τ decay channel in detail.

Concerning the effect of systematic uncertainties, we point out that the experimental resolutions considered in our MC study reduce the significances for observing entanglement and Bell inequality violation by rather moderate amounts of 10% and 30%, respectively. Since systematic uncertainties refer to uncertainties on the experimental resolutions and on the background, we expect their effect to be comparable in size to the effect of the experimental resolutions and of the background. If systematic uncertainties constitute a limiting factor to the sensitivity of the analysis, we expect that their effect can be mitigated by including suitable control regions into the ML fit or by auxiliary measurements, taking advantage of the large dataset of $e^+e^- \to \tau^+\tau^-$ events recorded by Belle II.

We expect non-Gaussian tails to affect the numerical values of the significances but not to alter our conclusion that an observation of entanglement and Bell inequality violation with a significance well in excess of five s.d. is highly likely once the Belle II Collaboration reproduces our study with their data.

In summary, we are confident that the presence of non-Gaussian tails in the experimental resolutions, backgrounds, and systematic uncertainties disregarded in our analysis will not prevent the observation of entanglement and Bell inequality violation in the process $e^+e^- \to \tau^+\tau^-$ at Belle II.

VI. SUMMARY

We have studied the prospects for testing quantum mechanics by probing entanglement and Bell inequality violation in the process $e^+e^- \to \tau^+\tau^-$ at Belle II. We expect that a dataset of 200 million $e^+e^- \to \tau^+\tau^-$ events will be sufficient to observe quantum entanglement and Bell inequality violation with a significance well in excess of five standard deviations after full detector effects, backgrounds, and systematic uncertainties are taken into account. A dataset of this size has already been recorded by Belle II.

Our study is based on the analysis of six decay channels: $\pi^+\pi^-$, $\pi^\pm\rho^\mp$, $\pi^\pm a_1^\mp$, $\rho^+\rho^-$, $\rho^\pm a_1^\mp$, and $a_1^+a_1^-$. Compared to analyzing only the decay channel $\pi^+\pi^-$, the channel most prominently studied in the context of τ spin measurements in the literature, the combination of all six decay channels improves the significance for detecting entanglement by more than a factor of 4 and the significance for detecting Bell inequality violation by more than a factor of 2. The inclusion of the decay channels $\pi^\pm\rho^\mp$, $\pi^\pm a_1^\mp$, $\rho^+\rho^-$, $\rho^\pm a_1^\mp$, and $a_1^+a_1^-$ into the analysis will be possible if the charged and neutral pions produced in the τ decays can be reconstructed with high efficiency and purity.

We encourage the Belle II Collaboration to reproduce this study with their full detector simulation and their data.

ACKNOWLEDGMENTS

L. M. is supported by the Estonian Research Council Grants PRG356 and RVTT3. K. E. and C. V. are supported by the Estonian Research Council Grant No. PRG445. We thank Kristjan Kannike for useful discussions, the Galileo Galilei Institute for Theoretical Physics for the hospitality, and the INFN for partial support during the completion of this work.

APPENDIX A: ANALYTIC EQUATIONS FOR KINEMATIC RECONSTRUCTION

The formalism introduced in Appendix C in Ref. [46] yields approximate values for the eight unknown components of the τ^+ and τ^- four-vectors by applying eight constraints and solving the resulting system of linear equations. Two constraints refer to the mass of the τ lepton four-vector, and two require the neutrinos to be massless. The remaining four constraints are obtained by demanding the four-vector of the $\tau^+\tau^-$ system to be equal to the initial state of the e^+e^- collision: $p_{\tau\tau} = (E_{e^+} + E_{e^-}, 0, 0, E_{e^-} - E_{e^+})$, where E_{e^+} and E_{e^-} refer to the nominal energies of the e^+ and e^- beams, respectively, and the z axis points in direction of the electron beam. We have extended the formalism to the case of arbitrary hadronic τ decay channels, obtaining the following relations, which we use in lieu of the equations given in Appendix C in Ref. [46].

We start by parametrizing the four-vectors of the τ^+ and τ^-, denoted by the symbols p_{τ^+} and p_{τ^-}, by

$$p^\mu_{\tau^\pm} = \frac{1 \mp a}{2} p_{\tau\tau} \pm \frac{b}{2} p^\mu_{h^+} \mp \frac{c}{2} p^\mu_{h^-} \pm d q_\mu, \quad \text{(A1)}$$

where

$$q^{\mu} = \frac{1}{s}\epsilon^{\mu}{}_{\nu\rho\sigma} p^{\nu}_{\tau\tau} p^{\rho}_{h^+} p^{\sigma}_{h^-} \tag{A2}$$

and the symbols a, b, c, and d represent four coefficients, which are to be determined. The first three of the coefficients, a, b, and c, are obtained as solutions to the equation

$$\begin{pmatrix} a \\ b \\ c \end{pmatrix} = [M]^{-1} \cdot \mathbf{\Lambda}, \tag{A3}$$

where

$$[M] = \begin{pmatrix} -x & m^2_{h^+} & -z \\ y & -z & m^2_{h^-} \\ s & -x & y \end{pmatrix} \quad \text{and} \quad \mathbf{\Lambda} = \begin{pmatrix} m^2_{\tau} + m^2_{h^+} - x \\ m^2_{\tau} + m^2_{h^-} - y \\ 0 \end{pmatrix}. \tag{A4}$$

In the above equations, the symbols p_{h^+} and p_{h^-} denote the momentum of the τ^+_{h} and τ^-_{h}, i.e., the momentum of the system of $\pi^{\pm}$ and γ produced in the decays of the τ^+ and τ^-, and m_{h^+} and m_{h^-} denote the masses of these systems. The symbol s denotes the square of the center-of-mass energy of 10.579 GeV and $\epsilon^{\mu\nu\rho\sigma}$ the Levi-Civita tensor. The symbols x, y, and z are defined, respectively, by

$$x = p_{\tau\tau} \cdot p_{h^+}, \quad y = p_{\tau\tau} \cdot p_{h^-}, \text{ and } z = p_{h^+} \cdot p_{h^-}. \tag{A5}$$

The fourth coefficient, d, is given by

$$d^2 = -\frac{1}{4q^2}[(1+a^2)s + b m^2_{h^+} + c m^2_{h^-} - 4m^2_{\tau} + 2(acy - abx - bcz)]. \tag{A6}$$

Equation (A6) yields two solutions of opposite sign, which determine the four-vectors p_{τ^+} and p_{τ^-} up to a twofold sign ambiguity. We resolve the sign ambiguity by choosing the solution more compatible with tracking information [71]. For the decay channels $\pi^{\pm}$ and $\rho^{\pm}$, we quantify the level of compatibility based on the transverse impact parameter of the charged pion's track, while for the decay channel $\mathrm{a}^{\pm}_1$ we use the position of the τ decay vertex.

APPENDIX B: COMPARISON OF DIFFERENT METHODS FOR MEASURING SPIN CORRELATION

Alternatively to the ML fit given by Eq. (4.5), the polarization vectors $\mathbf{B}^+$ and $\mathbf{B}^-$ for the τ^+ and τ^- and the spin correlation matrix $\mathbf{C}$ can be measured by the following.

1. Expectation value

Reference [46] uses the expectation values of the product of the polarimeter vectors $\mathbf{h}^+$ and $\mathbf{h}^-$ to measure the elements of $\mathbf{B}^+$, $\mathbf{B}^-$, and $\mathbf{C}$. The relation between the expectation values of $\mathbf{h}^{\pm}$ and $\mathbf{B}^{\pm}$ and between $\langle \mathbf{h}^+ \cdot \mathbf{h}^- \rangle$ and $\mathbf{C}$ is given by Eq. (30) of Ref. [46]. It reads

$$\begin{aligned} \mathbf{B}^{\pm}_i &= 3\langle \mathbf{h}^{\pm}_i \rangle, \\ \mathbf{C}_{ij} &= 9\langle \mathbf{h}^+_i \mathbf{h}^-_j \rangle, \end{aligned} \tag{B1}$$

where the indices i and j are either n, r, or k and the expectation value is computed as the average over the events in the $\mathrm{e}^+\mathrm{e}^- \to \tau^+\tau^-$ event sample.

2. Double-differential cross section

Expressing the Lorentz invariant phase-space measure in Eq. (4.4) in polar coordinates and integrating over the azimuthal angles ϕ^+ and ϕ^- yields the following expression for the double-differential (2d) cross section as a function of the polar angles θ^+ and θ^-, given by Eq. (VI.6) in Ref. [72]:

$$\frac{1}{\sigma}\frac{d\sigma}{d\cos\theta^+_i d\cos\theta^-_j} = \frac{1}{4}(1 + \mathbf{C}_{ij}\cos\theta^+_i \cos\theta^-_j), \tag{B2}$$

where $\cos\theta^+_i = \mathbf{h}^+ \cdot \hat{e}_i$ ($\cos\theta^+_j = \mathbf{h}^+ \cdot \hat{e}_j$) denotes the direction cosine of the polarimetric vector $\mathbf{h}^+$ ($\mathbf{h}^-$) with one of the basis vectors $\{\hat{\mathbf{n}}, \hat{\mathbf{r}}, \hat{\mathbf{k}}\}$ in the rest frame of the τ^+ (τ^-) and $i, j \in \{n, r, k\}$.

3. Single-differential cross section

The spin correlation matrix $\mathbf{C}$ may alternatively be extracted from the single-differential (1d) cross section as a function of the observable $\xi_{ij} = \cos\theta^+_i \cos\theta^-_j$, given by Eq. (4.16) in Ref. [73]:

$$\frac{1}{\sigma}\frac{d\sigma}{d\xi_{ij}} = \frac{1}{2}(1 + \mathbf{C}_{ij}\xi_{ij}) \ln\left(\frac{1}{|\xi|}\right). \tag{B3}$$

4. Forward-backward asymmetry

Alternatively, one may extract the τ spin correlation using the forward-backward (FB) asymmetries given by Eq. (25) in Ref. [30]:

$$\begin{aligned} A_{ij} &= \frac{N(\cos\theta^+_i \cos\theta^-_j > 0) - N(\cos\theta^+_i \cos\theta^-_j < 0)}{N(\cos\theta^+_i \cos\theta^-_j > 0) + N(\cos\theta^+_i \cos\theta^-_j < 0)} \\ &= \frac{1}{4}\mathbf{C}_{ij}, \end{aligned} \tag{B4}$$

where the symbol N represents number of events, the direction cosines $\cos\theta^+_i$ and $\cos\theta^-_j$ are defined as before, and $i, j \in \{n, r, k\}$.

In case of the double-differential (single-differential) cross section, binned distributions in θ_i^+ versus θ_j^- (ξ_{ij}) are fitted to determine the element $\mathbf{C}_{ij}$ of the spin correlation matrix. The fits are implemented using the software package RooFit [74].

Different conventions exist in the literature for defining the helicity frame and the sign of the polarimeter vector. These conventions lead to different signs for the terms proportional to $\mathbf{B}_i^{\pm}$ and $\mathbf{C}_{ij}$ in Eqs. (B1)–(B4). The signs in the equations above match our definition of the helicity frame and of the polarimeter vector.

The sensitivity of the different methods is compared in Table IV. The ML-fit method provides the lowest uncertainties and, thus, the highest significance. While the performance of the fits to binned 2D and 1D cross sections comes close to the performance of the ML-fit method, the significances for the expectation value and forward-backward asymmetry methods are about 15% and 30% lower. The performance advantage of the unbinned ML fit increases if the size of the event sample is reduced.

TABLE IV. Observables $\mathcal{C}[\rho]$ and $\mathfrak{m}_{12}[\mathbf{C}]$ measured in the combination of decay channels $\pi^+\pi^-$, $\pi^{\pm}\rho^{\mp}$, $\pi^{\pm}a_1^{\mp}$, $\rho^+\rho^-$, $\rho^{\pm}a_1^{\mp}$, and $a_1^+a_1^-$, for events that pass the selection $|\cos(\vartheta)| < 0.40$. Events are analyzed on MC-truth level. No acceptance cuts are applied on the $\pi^{\pm}$ and γ produced in the τ decays.

Method	$\mathcal{C}[\rho]$	$\mathfrak{m}_{12}[\mathbf{C}]$
Expected value	0.6952 ± 0.0013	1.4270 ± 0.0037
2D distribution	0.6950 ± 0.0013	1.4331 ± 0.0032
1D distribution	0.6949 ± 0.0012	1.4253 ± 0.0033
FB asymmetry	0.6932 ± 0.0017	1.4315 ± 0.0045
ML fit	0.6952 ± 0.0011	1.4283 ± 0.0031

[1] J. S. Bell, On the Einstein-Podolsky-Rosen paradox, Phys. Phys. Fiz. **1**, 195 (1964).
[2] N. Brunner, D. Cavalcanti, S. Pironio, V. Scarani, and S. Wehner, Bell nonlocality, Rev. Mod. Phys. **86**, 419 (2014).
[3] A. Aspect, J. Dalibard, and G. Roger, Experimental test of Bell's inequalities using time varying analyzers, Phys. Rev. Lett. **49**, 1804 (1982).
[4] G. Weihs, T. Jennewein, C. Simon, H. Weinfurter, and A. Zeilinger, Violation of Bell's inequality under strict Einstein locality conditions, Phys. Rev. Lett. **81**, 5039 (1998).
[5] J. F. Clauser, M. A. Horne, A. Shimony, and R. A. Holt, Proposed experiment to test local hidden variable theories, Phys. Rev. Lett. **23**, 880 (1969).
[6] J. F. Clauser and M. A. Horne, Experimental consequences of objective local theories, Phys. Rev. D **10**, 526 (1974).
[7] B. Hensen *et al.*, Loophole-free Bell inequality violation using electron spins separated by 1.3 kilometres, Nature (London) **526**, 682 (2015).
[8] M. Giustina *et al.*, Significant-loophole-free test of Bell's theorem with entangled photons, Phys. Rev. Lett. **115**, 250401 (2015).
[9] S. Storz *et al.*, Loophole-free Bell inequality violation with superconducting circuits, Nature (London) **617**, 265 (2023).
[10] W. Rosenfeld, D. Burchardt, R. Garthoff, K. Redeker, N. Ortegel, M. Rau, and H. Weinfurter, Event-ready Bell test using entangled atoms simultaneously closing detection and locality loopholes, Phys. Rev. Lett. **119**, 010402 (2017).
[11] J. F. Clauser and A. Shimony, Bell's theorem: Experimental tests and implications, Rep. Prog. Phys. **41**, 1881 (1978).
[12] M. Genovese, Research on hidden variable theories: A review of recent progresses, Phys. Rep. **413**, 319 (2005).
[13] M. Lamehi-Rachti and W. Mittig, Quantum mechanics and hidden variables: A test of Bell's inequality by the measurement of the spin correlation in low-energy proton–proton scattering, Phys. Rev. D **14**, 2543 (1976).
[14] N. A. Tornqvist, Suggestion for Einstein-Podolsky-Rosen experiments using reactions like $e^+e^- \to \Lambda\bar{\Lambda} \to \pi^- p \pi^+ \bar{p}$, Found. Phys. **11**, 171 (1981).
[15] S. A. Abel, M. Dittmar, and H. K. Dreiner, Testing locality at colliders via Bell's inequality?, Phys. Lett. B **280**, 304 (1992).
[16] F. Benatti and R. Floreanini, Bell's locality and ε'/ε, Phys. Rev. D **57**, R1332 (1998).
[17] F. Benatti and R. Floreanini, *CP*-violation as a test of quantum mechanics, Eur. Phys. J. C **13**, 267 (2000).
[18] R. A. Bertlmann, W. Grimus, and B. C. Hiesmayr, Bell inequality and *CP* violation in the neutral kaon system, Phys. Lett. A **289**, 21 (2001).
[19] S. Banerjee, A. K. Alok, and R. MacKenzie, Quantum correlations in B and K meson systems, Eur. Phys. J. Plus **131**, 129 (2016).
[20] A. Acin, J. I. Latorre, and P. Pascual, Three party entanglement from positronium, Phys. Rev. A **63**, 042107 (2001).
[21] A. Go (Belle Collaboration), Observation of Bell inequality violation in B mesons, J. Mod. Opt. **51**, 991 (2004).
[22] S. P. Baranov, Bell's inequality in charmonium decays $\eta_c \to \Lambda\bar{\Lambda}$, $\chi_c \to \Lambda\bar{\Lambda}$ and $J/\psi \to \Lambda\bar{\Lambda}$, J. Phys. G **35**, 075002 (2008).
[23] S. Banerjee, A. K. Alok, R. Srikanth, and B. C. Hiesmayr, A quantum information theoretic analysis of three flavor neutrino oscillations, Eur. Phys. J. C **75**, 487 (2015).
[24] N. Yongram and E. B. Manoukian, Quantum field theory analysis of polarizations correlations, entanglement and Bell's inequality: explicit processes, Fortschr. Phys. **61**, 668 (2013).
[25] A. Cervera-Lierta, J. I. Latorre, J. Rojo, and L. Rottoli, Maximal entanglement in high energy physics, SciPost Phys. **3**, 036 (2017).

[26] Y. Afik and J. R. M. de Nova, Entanglement and quantum tomography with top quarks at the LHC, Eur. Phys. J. Plus **136**, 907 (2021).

[27] M. Fabbrichesi, R. Floreanini, and G. Panizzo, Testing Bell inequalities at the LHC with top-quark pairs, Phys. Rev. Lett. **127**, 161801 (2021).

[28] C. Severi, C. D. E. Boschi, F. Maltoni, and M. Sioli, Quantum tops at the LHC: From entanglement to Bell inequalities, Eur. Phys. J. C **82**, 285 (2022).

[29] A. J. Larkoski, General analysis for observing quantum interference at colliders, Phys. Rev. D **105**, 096012 (2022).

[30] J. A. Aguilar-Saavedra and J. A. Casas, Improved tests of entanglement and Bell inequalities with LHC tops, Eur. Phys. J. C **82**, 666 (2022).

[31] Y. Afik and J. R. M. de Nova, Quantum discord and steering in top quarks at the LHC, Phys. Rev. Lett. **130**, 221801 (2023).

[32] Y. Afik and J. R. M. de Nova, Quantum information with top quarks in QCD, Quantum **6**, 820 (2022).

[33] W. Gong, G. Parida, Z. Tu, and R. Venugopalan, Measurement of Bell-type inequalities and quantum entanglement from Λ-hyperon spin correlations at high energy colliders, Phys. Rev. D **106**, L031501 (2022).

[34] A. J. Barr, Testing Bell inequalities in Higgs boson decays, Phys. Lett. B **825**, 136866 (2022).

[35] J. A. Aguilar-Saavedra, A. Bernal, J. A. Casas, and J. M. Moreno, Testing entanglement and Bell inequalities in $H \to ZZ$, Phys. Rev. D **107**, 016012 (2023).

[36] R. Ashby-Pickering, A. J. Barr, and A. Wierzchucka, Quantum state tomography, entanglement detection and Bell violation prospects in weak decays of massive particles, J. High Energy Phys. 05 (2023) 020.

[37] M. Fabbrichesi, R. Floreanini, E. Gabrielli, and L. Marzola, Bell inequalities and quantum entanglement in weak gauge bosons production at the LHC and future colliders, Eur. Phys. J. C **83**, 823 (2023).

[38] G. Aad *et al.* (ATLAS Collaboration), Observation of quantum entanglement in top-quark pairs using the ATLAS detector, arXiv:2311.07288.

[39] M. Fabbrichesi, R. Floreanini, E. Gabrielli, and L. Marzola, Bell inequality is violated in $B^0 \to J/\psi K^*(892)^0$ decays, arXiv:2305.04982.

[40] D. Sahoo *et al.* (Belle Collaboration), Search for lepton-number- and baryon-number-violating tau decays at Belle, Phys. Rev. D **102**, 111101 (2020).

[41] Belle-II Collaboration, Measurement of the τ-lepton mass with the Belle II experiment, Phys. Rev. D **108**, 032006 (2023).

[42] SuperKEKB Collaboration, SuperKEKB Collider, Nucl. Instrum. Methods Phys. Res., Sect. A **907**, 188 (2018).

[43] W. Altmannshofer *et al.* (Belle-II Collaboration), The Belle II physics book, Prog. Theor. Exp. Phys. **2019**, 123C01 (2019); **2020**, 029201(E) (2020).

[44] P. Privitera, Decay correlations in $e^+e^- \to \tau^+\tau^-$ as a test of quantum mechanics, Phys. Lett. B **275**, 172 (1992).

[45] M. Fabbrichesi, R. Floreanini, and E. Gabrielli, Constraining new physics in entangled two-qubit systems: Top-quark, tau-lepton and photon pairs, Eur. Phys. J. C **83**, 162 (2023).

[46] M. M. Altakach, P. Lamba, F. Maltoni, K. Mawatari, and K. Sakurai, Quantum information and *CP* measurement in $H \to \tau^+\tau^-$ at future lepton colliders, Phys. Rev. D **107**, 093002 (2023).

[47] K. Ma and T. Li, Testing Bell inequality through $H \to \tau\tau$ at CEPC, arXiv:2309.08103.

[48] W. Bernreuther, A. Brandenburg, Z. G. Si, and P. Uwer, Top quark spin correlations at hadron colliders: Predictions at next-to-leading order QCD, Phys. Rev. Lett. **87**, 242002 (2001).

[49] C. Bouchiat and L. Michel, Mesure de la polarisation des electrons relativistes, Nucl. Phys. **5**, 416 (1958).

[50] C. H. Bennett, D. P. DiVincenzo, J. A. Smolin, and W. K. Wootters, Mixed state entanglement and quantum error correction, Phys. Rev. A **54**, 3824 (1996).

[51] R. Horodecki, P. Horodecki, M. Horodecki, and K. Horodecki, Quantum entanglement, Rev. Mod. Phys. **81**, 865 (2009).

[52] W. K. Wootters, Entanglement of formation of an arbitrary state of two qubits, Phys. Rev. Lett. **80**, 2245 (1998).

[53] J. F. Clauser and A. Shimony, Bell's theorem. Experimental tests and implications, Rep. Prog. Phys. **41**, 1881 (1978).

[54] R. Horodecki, P. Horodecki, and M. Horodecki, Violating bell inequality by mixed spin-12 states: Necessary and sufficient condition, Phys. Lett. A **200**, 340 (1995).

[55] J. S. Bell, *Spekable and Unspeakable in Quantum Mechanics. Collected Papers on Quantum Philosophy* (Cambridge University Press, Cambridge, England, 1987).

[56] S. Jadach, J. H. Kühn, and Z. Was, TAUOLA: A library of Monte Carlo programs to simulate decays of polarized tau leptons, Comput. Phys. Commun. **64**, 275 (1990).

[57] V. Cherepanov and C. Veelken, The polarimeter vector for $\tau \to 3\pi\nu_\tau$ decays, arXiv:2311.10490.

[58] J. H. Kühn, Tau polarimetry with multi-meson states, Phys. Rev. D **52**, 3128 (1995).

[59] M. Davier, L. Duflot, F. Le Diberder, and A. Rouge, The optimal method for the measurement of tau polarization, Phys. Lett. B **306**, 411 (1993).

[60] R. J. Rossi, *Mathematical Statistics: An Introduction to Likelihood Based Inference* (John Wiley & Sons, New York, 2018).

[61] F. James and M. Roos, MINUIT: A system for function minimization and analysis of the parameter errors and correlations, Comput. Phys. Commun. **10**, 343 (1975).

[62] J. Alwall, R. Frederix, S. Frixione, V. Hirschi, F. Maltoni, O. Mattelaer, H. S. Shao, T. Stelzer, P. Torrielli, and M. Zaro, The automated computation of tree-level and next-to-leading order differential cross sections, and their matching to parton shower simulations, J. High Energy Phys. 07 (2014) 079.

[63] C. Bierlich *et al.*, A comprehensive guide to the physics and usage of PYTHIA 8.3 SciPost Phys. Codeb. **2022**, 8 (2022), 10.21468/SciPostPhysCodeb.8.

[64] Belle-II Collaboration, Belle II technical design report, arXiv:1011.0352.

[65] GEANT4 Collaboration, Geant4–A simulation toolkit, Nucl. Instrum. Methods Phys. Res., Sect. A **506**, 250 (2003).

[66] P. Avery, Fitting theory writeups and references, https://www.phys.ufl.edu/~avery/fitting.html.
[67] P. Sauerland, Kinematic reconstruction of tau leptons and test for lepton universality in charged weak interactions with the CMS experiment, Ph.D. thesis, RWTH Aachen, 2011, https://cds.cern.ch/record/1358627.
[68] V. Cherepanov and A. Zotz, Kinematic reconstruction of $Z/H \to \tau\tau$ decay in proton-proton collisions, arXiv:1805.06988.
[69] P. Avery, Applied fitting theory I—general least squares theory, https://www.phys.ufl.edu/~avery/fitting/fitting1.pdf.
[70] B. Efron, Bootstrap methods: Another look at the Jackknife, Ann. Stat. **7**, 1 (1979).
[71] J. H. Kühn, Tau kinematics from impact parameters, Phys. Lett. B **313**, 458 (1993).
[72] W. Bernreuther, A. Brandenburg, Z. G. Si, and P. Uwer, Top quark pair production and decay at hadron colliders, Nucl. Phys. **B690**, 81 (2004).
[73] W. Bernreuther, D. Heisler, and Z.-G. Si, A set of top quark spin correlation and polarization observables for the LHC: Standard Model predictions and new physics contributions, J. High Energy Phys. 12 (2015) 026.
[74] W. Verkerke and D. P. Kirkby, The RooFit toolkit for data modeling, eConf **C0303241**, MOLT007 (2003), arXiv:physics/0306116.